Persistent photocurrent decay mechanisms by capture of photoelectrons in GaAs-$Al_xGa_{1-x}As$ heterostructures

L. X. He, K. P. Martin,* and R. J. Higgins*
Department of Physics, University of Oregon, Eugene, Oregon 97403
(Received 9 February 1987; revised manuscript received 28 May 1987)

We introduce a method for separating multiple-rate decay mechanisms of persistent photoconductivity (PPC) in GaAs/$Al_xGa_{1-x}As$ heterostructures. The derivative of the decay of measured conductivity or carrier number density with respect to the logarithm of time (1 msec–1000 sec) shows a slowly varied base-line structure with some pronounced peaks. The temperature dependence of the varied base line agrees with the temperature dependence of the tunneling barrier. The temperature dependence of the base-line structure and the positions of the pronounced peaks was analyzed to yield capture energies and corresponding lifetime prefactors. The collected evidence demonstrates that the combination of measured capture energies and lifetime prefactors can distinguish the microscopic contributions to PPC decay in the doped $Al_xGa_{1-x}As$ layer of samples from other capture mechanisms. (1) The short-lifetime prefactor (10^{-8}–10^{-10} sec) and associated capture energies are in good agreement with the results from other work on the *DX*-center capture mechanism. (2) This short-lifetime prefactor in a narrow range of temperature compares with prefactors longer by as much as 10 orders of magnitude in adjacent ranges of temperature, which can be identified as tunneling related PPC decay of the two-dimensional electron gas into shallow or deep donors in the $Al_xGa_{1-x}As$ layer. (3) The mechanism with short-lifetime prefactors cannot lie on the GaAs side of the heterojunction because of the observed strong gate-bias dependence and doping-density dependence of the decay magnitude.

I. INTRODUCTION

Persistent photoconductivity (PPC) is known for many semiconductor materials and configurations.[1] Light-enhanced electrical conductivity, carrier concentration, and carrier mobility persist for times ranging from hours to days after the illumination is removed as long as the temperature is below about 100 K, and shorter-term memory is observed even at room temperature. It is important to understand PPC effects in modulation-doped materials and high-electron-mobility transistors (HEMT's) at temperatures below 100 K at which HEMT's display optimal electronic properties. An understanding of PPC effects also contributes to the control of the mechanisms behind current collapse (a change from high to low conductivity following biasing past a certain threshold) and backgating effects (the sensitivity of conductivity in one transistor structure to bias in an adjacent structure) which may have related origins. While in bulk materials or single-layer devices there is some agreement that PPC is related to photoionization of deep levels which have a recombination barrier, a diverse collection of models has been proposed to explain the interplay between *macroscopic* (band-bending) and *microscopic* (deep-level) mechanisms in the layered HEMT structure. This paper is a contribution to separating the dominant mechanisms for PPC-associated decay in HEMT structures from among the two distinct approaches which have been suggested (summarized qualitatively in Fig. 1).

1. Macroscopic-barrier (band-bending) models. The macroscopic-barrier theory[2] involves the spatial separation of photogenerated electrons and holes by built-in electric fields from macroscopic potential barriers due to band bending at surfaces, heterostructure interfaces, or doping profiles. In the case of the $Al_xGa_{1-x}As$/GaAs

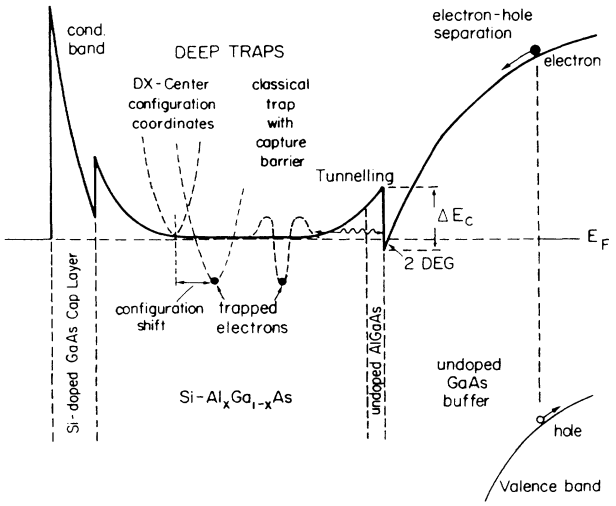

FIG. 1. Major models for persistent photocurrent in HEMT structures, including macroscopic-barrier (band-bending induced electron-hole separation) model and microscopic-barrier (deep-level) models.

heterostructure, this persistence mechanism takes place predominantly in the GaAs side, where the built-in field configuration provides both a mechanism to sweep out photogenerated holes and an electron collection region, the two-dimensional electron gas (2D EG) of the HEMT. Recombination requires that an electron be thermally activated to reach an available hole or hole trap in the GaAs substrate or flat-band region, and requires a time τ:

$$\tau=\tau_r \exp(E_B/kT) , \tag{1}$$

where τ_r is the recombination time without the potential barrier, and is determined by other relatively temperature-insensitive decay processes in the recombination sequence, and E_B is the height of the macroscopic barrier. If these effective potential barriers E_B are sufficiently high in comparison to kT, the recombination time τ can become extremely long, since

$$E_B/kT=E_{\text{gap}}(\text{GaAs})/2kT$$
$$=(1.4\text{ eV})/(0.02\text{ eV})=70$$

at 100 K, for example. If traps are present in the substrate or epitaxially grown GaAs buffer region, a distribution of lower values of E_B can be anticipated.

The electron-hole separation mechanism is not considered in the $Al_xGa_{1-x}As$ layer and the cap layer. In this case, the separated holes will move towards either the 2D EG or metal gate (or surface in the ungated case) where some electrons states are always present.

Tunneling[3] also provides a mechanism for electrons to move between the $Al_xGa_{1-x}As$ and GaAs layers despite the macroscopic barrier presented by the conduction band. The lifetime of the tunneling-assisted capture is determined by the tunneling probability and the local capture cross section after tunneling. The local capture cross section of ionized donors is strongly temperature dependent for the case of deep traps, but is only weakly temperature dependent for the case of shallow traps. When kT is much smaller than the height of the tunneling barrier, the Wentzel-Kramers-Brillouin (WKB) method shows the tunneling probability only depends on the shape of the tunneling barrier.

Consider a typical tunneling barrier $U=U(z)$ shown in Fig. 2, where the 2D interface is on the [100] direction and the ionized donors are located in layers parallel to the 2D interface. In the case of $Al_xGa_{1-x}As$, these atomic donor layers are of distance $d=0.283$ nm from each other. After tunneling but before capture, an electron has the same energy as at the 2D interface. For a fixed temperature, the capture after tunneling would be the same for different tunneling distances assuming the local ionized donors have the same capture cross section. Under this assumption, the difference in the tunneling probabilities of an electron reaching different layers will determine the difference of the overall decay lifetime. By the WKB approximation, the probability of an electron reaching the layer $z=z_0$ (Fig. 2) is (the kinetic energy of the electron being ignored)

$$P=\exp\left[\int_0^{z_0}(4\pi/h)(2m^*U)^{1/2}dz\right] , \tag{2}$$

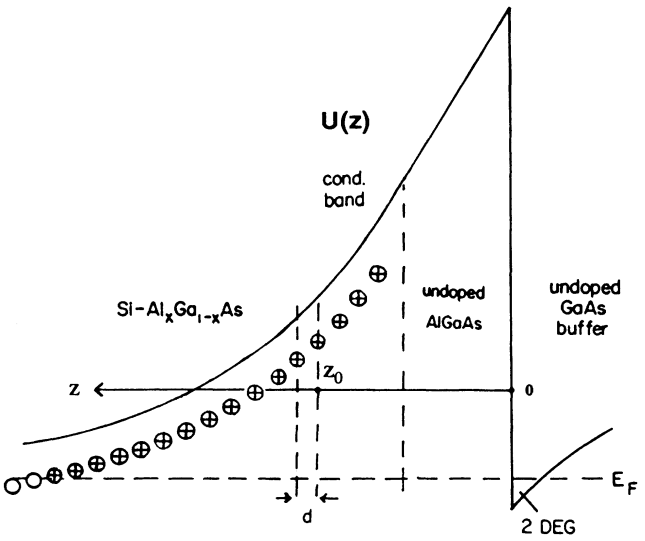

FIG. 2. Typical tunneling barrier for a $GaAs/Al_xGa_{1-x}As$ heterostructure.

where m^* is the effective mass of an electron in the $Al_xGa_{1-x}As$ layer. Because the separation d of atomic planes in the donor layer is much smaller than the typical depletion width (30 nm), and assuming that the overall barrier is nearly the same for an electron reaching the layer at $z=z_0+d$ as for $z=z_0$, then the ratio of the lifetime of an electron captured by the ionized donors in adjacent atomic layers is

$$R=\exp[(4\pi/h)(2m^*U_0)^{1/2}d] , \tag{3}$$

where U_0 is the potential barrier height at these adjacent layers. Setting $m^*=0.092m_0$ for an Al fraction $x=0.3$, we have

$$R=\exp(0.879U_0^{1/2}) , \tag{4}$$

where U_0 is in eV. For example, when U_0 is 0.15 eV, R is 1.4.

When the shape of the tunneling barrier is known (by the depletion approximation), the lifetime for tunneling-assisted capture into each donor layer can therefore be expressed in terms of the lifetime of a 2D EG electron captured by an ionized donor in the first layer from the 2D EG.

Due to the small tunneling probability through the undoped spacer layer between the GaAs and doped $Al_xGa_{1-x}As$ (typically 10^{-4} for a barrier with a 0.3 eV height and 5 nm width) the lifetime of tunneling-assisted capture (even to reach the first layer of ionized donors) is much longer than the decay lifetime by direct capture assuming the same local capture cross section for the ionized donors. The direct-capture lifetime by a shallow donor is of the order of 1 msec at $T=100$ K, but the lifetime for direct capture by a deep donor is of the order of 1000 sec or more at the same temperature. Therefore, for temperatures below 100 K, the observable tunneling-assisted capture through the undoped

$Al_xGa_{1-x}As$ layer within the time window of 1–1000 sec is likely to be shallow-donor related.

2. Microscopic-barrier (deep-level) models. Microscopic-barrier models[4,5] are based on postulated atomic-scale barriers that suppress recombination. The carriers in this case are photoexcited from the impurity center, a deep-donor complex (predominantly identified as the *DX* center in the Si-doped $Al_xGa_{1-x}As$ case) with photon energies smaller than the band gap of the material. These deep donors are thought to be impurity-atom-plus-defect complexes with large lattice relaxations, yielding large Stokes shifts: e.g., $E_{\text{optical}}=0.8$ eV while $E_{\text{thermal}}=0.15$ eV for $Al_xGa_{1-x}As$ with $x=0.35$. A configuration-coordinate model describes this situation. The empty deep level lies above the conduction-band minimum while the occupied deep level lies relatively deep within the gap with a large lattice relaxation required to shift between states. Recent work[6–10] has shown that such *DX* centers are tied to the *L* minimum of the $Al_xGa_{1-x}As$ conduction band. Under this picture, the apparent thermal capture energy must include the energy difference between the Γ and *L* minima.

A formula of the form (1) can also be used to estimate the microscopic barrier overcome during the retrapping of electrons by DX centers. The activation energy in formula (1) in this case is the capture energy E_c, and the prefactor τ_0 is mainly determined by the capture cross section in the high-temperature limit and was shown to be on the order of 10^{-10} sec for $0.27<x<0.35$ from a capture experiment.[11] Recapture dynamics due to deep-level microscopic barriers differ by orders of magnitude from those associated with macroscopic barriers and tunneling, which could also follow a decay curve of the form (1) but with a much longer lifetime prefactor. For example, in the case of shallow-donor capture after tunneling, the lifetime prefactor has been shown[3] to be of the order of 10 sec.

PPC decay kinetics need not be simply exponential. Unfortunately, a variety of mechanisms yield nonexponential decay, so that its observation does not identify a mechanism unambiguously.

(1) Deep-level transient spectroscopy (DLTS) measurements[12] show that both shallow centers and deep centers (*DX*) exist in $Al_xGa_{1-x}As$ layers, with a strong crossover from predominantly shallow donors to predominantly *DX* donors at about $x=0.2$. The *DX* center is found to have a distribution of energies,[13] so that activated capture will not necessarily yield simple exponential decay of PPC.

(2) For the $Al_xGa_{1-x}As/GaAs$ heterostructure, Schubert *et al.*[3] showed that PPC decays as a straight line when plotted against the logarithm of time and related this to their tunneling model. They found that the decay curve of a heterostructure at 4 K fits the tunneling model very well.

(3) Queisser and Theodorou[14] also predict a decay that is logarithmic in time due to the spatial distribution of distances between photoelectrons and recombination traps in the GaAs substrate layer.

In view of the variety of mechanisms available, extra information is needed to distinguish among decay mechanisms that contribute to the decay curve. In the work below, we demonstrate how our observed temperature dependence of decay time can be analyzed using a $\ln(t)$-derivative technique to yield a trap spectroscopy whose characteristic energies and times differ so significantly that direct capture (prefactors of 10^{-10} sec) and tunneling mechanisms (with prefactors of 1 sec) are unambiguously identifiable.

II. LOGARITHMIC DERIVATIVE OF MULTIPLE DECAY

The observation of multiple-rate decay behavior led to the use of a more sophisticated signal-processing method[15] in order to separate the temperature dependence of the decay due to each different mechanism.

Assume a general form of multiple-rate decay of the free-electron number density $N(t)$ at a fixed temperature T:

$$N(t)=\sum_i N_{i0}\exp(-t/t_i)\ , \tag{5}$$

where N_{i0} is the initial number density of decay channel i, and with a corresponding individual lifetime t_i.

The key results can be obtained with a more general multiple-rate form with an individual lifetime (t_i):

$$N(t)=\sum_i F(-t/t_i)\ . \tag{6}$$

Define a quantity $K(t)$, or so-called $\ln(t)$ derivative of N, by

$$\begin{aligned}K(t)&=-dN/d[\ln(t)]=-t dN/dt\\&=\sum_i (t/t_i)[dF(-t/t_i)/d(-t/t_i)]\ .\end{aligned} \tag{7}$$

For the moment consider the decay process over a narrow-enough temperature range T to T' so only one decay mechanism dominates, and all t_i can be expressed as (1) with same capture energy. This allows one to write down the following relation between t_i' and t_i:

$$t_i'=t_i\exp[(E/kT')-(E/kT)]\ , \tag{8}$$

where E is the capture energy, and t_i' is the new lifetime at T'.

At temperature T', replacing the lifetimes t_i in (7) by the new lifetimes t_i', we have a new $\ln(t)$ derivative of $N(t)$:

$$K'(t)=\sum_i (t/t_i')[dF(-t/t_i')/d(-t/t_i')]\ . \tag{9}$$

The time axis can be changed from t to a new time axis t' (i.e., make a change of time units) by

$$t=t'\exp[(E/kT')-(E/kT)]\ . \tag{10}$$

Notice that the individual lifetime t_i' is not altered by the change of the time axis. It is obvious from the above that $t/t_i'=t'/t_i$. Replacing t/t_i' in (9) by t'/t_i, we find that in the new time axis at temperature T'

$$K'(t)=K'(t')=\sum_i (t'/t_i)[dF(-t'/t_i)/d(-t'/t_i)]\ . \tag{11}$$

The right-hand side of (11) is the same form as (7) except that t is replaced by t'. A plot of (7) with $\ln(t)$ will be identical with a plot of (11) with $\ln(t')$. Because $\ln(t)=\ln(t')+[(E/kT')-(E/kT)]$, the plot of (9) with $\ln(t)$ must be simply displaced by $[(E/kT')-(E/kT)]$ from the plot of (7) with the same $\ln(t)$. Therefore, the capture energy E and the decay-time prefactor can be determined from the displacement measured by experiment.

For the simplest case of (5) with only a single decay lifetime t_0, such as direct capture by ionized donors in the doped supply layer,

$$K(t)=(t/t_0)N_{00}\exp(-t/t_0)\ . \tag{12}$$

The function is strongly peaked at precisely t_0, as shown in Fig. 3(a), with a peak value of N_{00}/e. We can measure the decay magnitude N_{00} from the peak value of $K(t)$. The half-width of the single decay peak in the $K(t)$-$\ln(t)$ plot is about one decade in time.

For the case of multiple-rate decay with the general form of (5), each decay channel is associated with a similar peak in $K(t)$ as its characteristic decay time. This forms the basis for a multiple-rate decay spectroscopy.

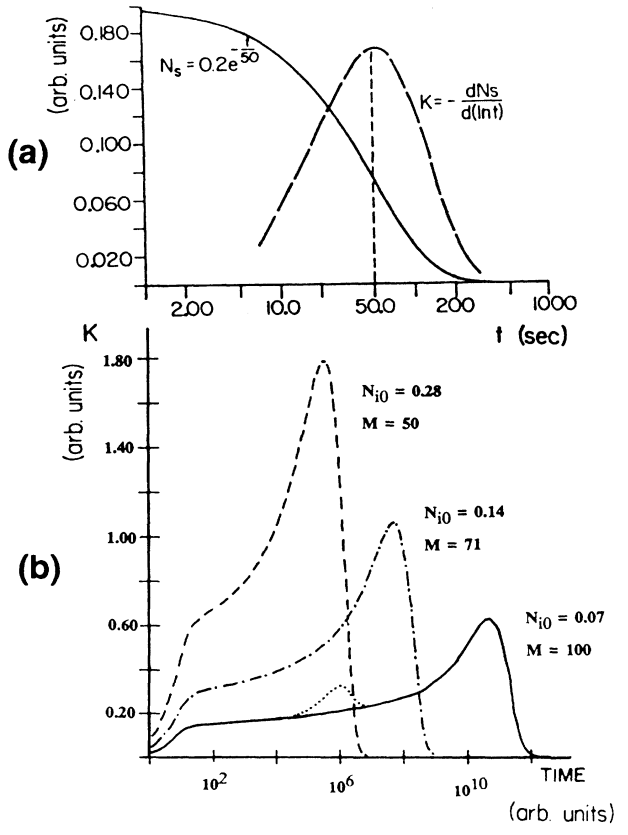

FIG. 3. Multiple-rate trap spectroscopy. (a) Any single exponential decay vs $\ln(t)$; the derivative (dashed line) displays a peak at the characteristic decay time. (b) A calculated result of $K(t)$ vs $\ln(t)$ of tunneling-assisted decay with different refilled ionized-donor densities N_{i0} and total number M of depleted donor-atom layers. The dotted curve at the bottom shows how a single isolated trap would superimpose.

From the definition of $K(t)$, we have

$$K(t)=\sum_i (t/t_i)N_{i0}\exp(-t/t_i)\ , \tag{13}$$

with peaks at $t=t_i^*$, where t_i^* can be slightly different from t_i. But when the assumption $t_i^*=t_i\exp[(E/kT')-(E/kT)]$ holds for a suitable temperature interval (N_{i0} is nearly constant in this temperature interval), from the general proof above, we can see that the peaks at t_i^* with a $\ln(t)$ plot shift from temperature T to a new temperature T' by $[(E/kT')-(E/kT)]$ in $\ln(t)$.

A linearlike plot of $N(t)$ versus $\ln(t)$ is obtained from expression (13) for a multiple-rate decay (5) with a certain form of the distribution of N_{i0}. As an example we consider the case of tunneling-assisted capture with a step-function tunneling barrier. From formula (2), the lifetime τ of an electron reaching a donor-atom layer is proportional to the exponential of the distance (z_0) from the 2D interface to this atomic donor layer. If N_{i0} has a continuous uniform distribution in the z direction in the doped layer, we have $dN=N_0\,d[\ln(\tau)]$ for fixed N_0. For an arbitrary time t within a given time window, when the longest lifetime (capture by the last donor-atom layer) and the shortest lifetime (capture by the first donor-atom layer) is far outside of the range of the time window, we have

$$K(t)=\int_0^\infty (t/\tau)(N_0/\tau)\exp(-t/\tau)d\tau=N_0\ . \tag{14}$$

$K(t)$ becomes a constant, and the plot of $N(t)$ with $\ln(t)$ will be a straight line. This conclusion also holds even for the more general form shown in (11).

For a well-separated multiple-rate decay process, $K(t)$ as determined from experimental decay data will show a sequence of peaks, with each peak corresponding to an individual decay channel in the multiple-rate process. Due to the broad half-width of a single decay channel in a $K(t)$-$\ln(t)$ plot, these peaks can be distinguished experimentally only when the separation is large enough. This condition is not generally satisfied for tunneling-assisted capture, because the difference in capture time between adjacent donor-atom layers is too small.

To investigate the behavior of tunneling-assisted decay with the realistic tunneling barrier, let us consider the simplest tunneling case shown in Fig. 2. Under the depletion approximation, the potential barrier height of the ith donor-atom layer can be expressed as

$$U_i=U_0(1-i/M)^2\ , \tag{15}$$

where M is the total number of the depleted donor atom layers and U_0 is the barrier height at the first layer. Using formula (3), all values of τ_i can be expressed in terms of τ_1, the lifetime of an electron captured by the first donor-atom layer, by the following iterative relation:

$$\tau_{i+1}=\tau_i\exp(0.879U_i^{1/2})\ . \tag{16}$$

Assuming a certain form of the distribution (N_{i0}) of ionized donors refilled by the tunneling electrons, the value of $K(t)$ can be calculated by formula (9).

A numerical simulation is shown in Fig. 3(b) using an arbitrary time unit that is determined by the lifetime of the tunneling-assisted capture into the first donor layer, and can be deduced from experimental data. In the solid curve, we assume 100 layers of donors with the same single-layer ionized-donor number density $N_{i0}=0.07$ (arbitrary units). The value of U_0 is chosen to be 0.3 eV, and the depletion width is the thickness of 100 donor-atom layers. The lifetime for the first layer is set to be 10 (arbitrary units). From the solid curve, we can see that $K(t)$ slowly increases over 10 orders of magnitude in time after initial capture by the first several layers begins until capture by the last few layers. Actually, the tunneling-assisted capture is a superposition of the capture contribution by each layer. The total result is the envelope of the superposition. The increasing slope up to the cutoff time has a physical explanation. When each layer makes the same contribution, the higher barrier at the first few layers in the depletion region nearest the 2D EG will have a bigger difference in the lifetime from adjacent layers. In this case, the peaks will be separated more from each other in a $\ln(t)$ plot, and have smaller overlap, giving smaller net $K(t)$ value. At larger time (further distance from the 2D interface) where the barrier becomes smaller, the small separation between peaks will show increased superposition, giving a higher $K(t)$ value. In this calculation, we ignore the possible nonuniform distribution of the single-layer ionized-donor number density. Otherwise, the real $K(t)$-$\ln(t)$ plot of tunneling-assisted decay may show additional fluctuations. But, with or without these fluctuations, the overall horizontal shift of the plot at the same values of $K(t)$ from different temperatures can be used to determine the activation energy and lifetime prefactor of capture by the local ionized donor. However, in fact, we will see that the temperature dependence of the ionization of donors at higher temperatures (typically above 100 K), and consequently different depletion lengths, will cause an extra shift of the tunneling-assisted decay curve. This is especially important when we interpret results for tunneling into the last few layers. In this case, although the tunneling may only be associated with shallow ionized donors, the decreasing tail of the $K(t)$-$\ln(t)$ plot [Fig. 3(b)] can have an extra shift towards a shorter time because of the decrease of the total number of tunneling layers. The dashed curves in Fig. 3(b) are the plots for the cases with larger $N_{i0}=0.14$ and 0.28 (same arbitrary units) and consequently shorter depletion length with a total of 71 and 50 layers of depleted donors, respectively. This is calculated by assuming that N_{i0} is proportional to the ionized-donor number density and the depletion width is determined by the depletion approximation. The lifetime for the tunneling-assisted capture into the first donor layer is set to be the same for the case of a shallow ionized donor. The plot shows clearly that the value of $K(t)$ for the capture into the first few donor layers is proportional to N_{i0}, and the time where the decreasing tail of the curve begins is strongly dependent on the depletion width. This strong shift is not from the change of the capture lifetime by the local ionized donors. The calculation shows that the amplitude of the central portion of the curve is about 3–10 times as large as the refilled ionized-donor number density of a single donor-atom layer. Considering that the fraction of refilled ionized donors out of the total ionized donors is of the order of a few percent, the amplitude of $K(t)$ for tunneling-assisted capture is of the order of the ionized-donor number density of a single donor-atom layer.

When the lifetime for direct capture into one type of ionized donor and the lifetime of tunneling-assisted capture into possibly another kind of donor is comparable within the same time window, the results of the mixture will depend on the amplitude of each kind of decay. If there are no, or very few, free carriers in the doped layer after illumination, we may not be able to distinguish any single decay peak in the plot of $K(t)$-$\ln(t)$, and tunneling-assisted capture will be the dominant decay mechanism. When their amplitudes are comparable, the slowly increasing base line will be augmented by a single peak [Fig. 3(b), dotted line]. At different temperatures, the shifts of the base line and the peak will be different if they correspond to different types of ionized donors. When the free-carrier density in the doped layer is much larger than the single-layer ionized-donor density, direct-capture decay can dominate, and the slowly increasing base line becomes less significant.

III. EXPERIMENTS AND DISCUSSION

Most of the molecular-beam-epitaxy (MBE) heterostructure samples in this work were composed of the following layer sequence: Si-doped GaAs cap layer, Si-doped $Al_xGa_{1-x}As$ layer, thin undoped $Al_xGa_{1-x}As$ spacer layer, thick undoped GaAs buffer layer, and semi-insulating GaAs substrate. A two-dimensional free-electron gas is formed at the interface between the undoped $Al_xGa_{1-x}As$ and GaAs buffer layers, separated by the spacer layer from the nearest donors in $Al_xGa_{1-x}As$ layer.

Samples from four different sources were used. Summarized in Table I are their principal parameters: aluminum fraction x, cap-layer thickness L_c, doping density $N_{d,c}$ of the cap layer, $Al_xGa_{1-x}As$-layer thickness L_a, $Al_xGa_{1-x}As$-layer doping density $N_{d,a}$, undoped spacer thickness L_s, gate voltage threshold (V_t) at 77 K in the dark, the net ionized-donor density N_i in the depleted $Al_xGa_{1-x}As$ layer at 77 K in the dark, and the percentage increase of N_i after identical brief white-light illumination, sufficient to saturate the PPC-induced change. Samples $A-C$ were gated samples. They are classic high-electron-mobility transistors. Samples A and B are on the same chip, and had $x=0.3$. Sample C had $x=0.21$. All metal gates are directly on top of the cap layer, which are not very heavily doped to ensure good gate characteristics. The samples with thick and heavily doped $Al_xGa_{1-x}As$ layers have free carriers in the $Al_xGa_{1-x}As$ layer when the gate bias is set higher than that required to deplete the doped supply layer (like that shown in Fig. 1). In this case, direct capture by an ionized donor will occur in the $Al_xGa_{1-x}As$ layer, and tunneling takes place through the undoped layer. Sam-

TABLE I. Sample label, source, aluminum ratio x, cap-layer thickness L_c, doping density $N_{d,c}$ of the cap layer, $Al_xGa_{1-x}As$-layer thickness L_a, $Al_xGa_{1-x}As$-layer doping density $N_{d,a}$, undoped spacer thickness L_s, gate voltage threshold V_t at 77 K in the dark, the net ionized-donor density N_i in the depleted $Al_xGa_{1-x}As$ layer at 77 K in the dark, and the percentage increase of N_i after identical brief white-light illumination sufficient to saturate the PPC change. Layer thicknesses are in units of nm and doping and carrier densities are in units of 10^{17} cm^{-3}.

Sample	Source	x	L_c (nm)	$N_{d,c}$	L_a (nm)	$N_{d,a}$	L_s (nm)	V_t (V)	N_i	$\Delta N_i/N_i$
A, B	Tek.[a]	0.3	50	2	100	10	5	−0.5	1.9	15%
C	TCSF[b]	0.21	20	6	120	6	8	−2.0	2.9	11%
D, DD	Cornell[c]	0.3	20	10	30	10	10	ungated	VDP	
G	Tek.[a]	0.3	50	2	100	10	5	ungated		
L	Gain[d]	0.3	30	20	50	15	4	ungated	VDP	

[a]Tek.: Tektronix Inc., Read Gleason and Richard Koyama.
[b]TCSF: Thomson-CSF (Paris), Paul Jay.
[c]Cornell: Cornell University, W. Schaff.
[d]Gain: Gain Electronics Corporation, T. Hurl.

ple *D*, an ungated van der Pauw (VDP) square, had $x=0.3$ in the Si-doped $Al_xGa_{1-x}As$ layer but $x=1.0$ in the undoped spacer layer, which makes for an extra-high tunneling barrier (1.0 eV). There is a 10 nm undoped $Al_xGa_{1-x}As$ layer ($x=0.3$) between the cap layer and doped $Al_xGa_{1-x}As$ layer. Sample *DD* has similar layer parameters and sample *L* (an ungated VDP) was chosen as a heavily doped sample in order that there be an extra large number of free carriers in the doped layer.

Gaps of 2–5 μm separate the gate from source or drain in our HEMT samples, and are sufficiently wide enough to prevent the gate voltage from influencing material under source and drain contact regions for small source-drain signals.[16] The source-drain voltage (V_{SD}) is kept below 1 meV to avoid hot-electron effects, and is much smaller than the smallest activation energy (>5 meV) involved.

All gated samples had a short enough gate length (1–2 μm) so that the diffused illumination could reach beneath the gate. This is proven by observed shifts in transconductance curves. In the charge-control picture,[17] the transconductance is low in the region where the gate controls only low-mobility carriers in the $Al_xGa_{1-x}As$ layer, and is much higher in the region where the gate controls the 2D EG number density. The transconductance peak occurs after the $Al_xGa_{1-x}As$ carrier density is depleted and the 2D EG is being modulated, and the pinchoff point occurs when the total carrier density at the 2D interface has been depleted. Shifts of the transconductance peak and the pinchoff threshold during the light illumination therefore give additional information about the changes of carrier densities in the different layers. Data from all gated samples at 77 K show large shifts (≥ 0.3 V) in the transconductance curves from their dark values following white light illumination, which relax back during the decay process towards their original form on very long time scales ($t>10^5$ sec). These measurements (which uniformly show a shift towards increased pinchoff-voltage magnitude) permit us to conclude unambiguously that light reached under the gate to increase the free-carrier density in the $Al_xGa_{1-x}As$ layer as well as the 2D EG.

For gated HEMT samples, the source-drain current I_{SD} was measured with V_{SD} fixed. For ungated van der Pauw samples, the carrier densities N_s were measured via the Hall effect. Both methods involve the number densities in the 2D and $Al_xGa_{1-x}As$ layers (N_{2D} and N_1) in a similar way.[18] When the mobility of 2D electrons (μ_{2D}) is much larger than the mobility of electrons in an $Al_xGa_{1-x}As$ layer (μ_1) such that $\mu_1 N_1 \ll \mu_{2D} N_{2D}$ (we ignore the difference between Hall mobility and conductance mobility because only the ratio μ_1/μ_{2D} is important in our case),

$$N_s = N_{2D} + 2N_1\mu_1/\mu_{2D} \text{ (Hall measurement)}, \quad (17)$$

$$I_{SD} = -eGV_{SD}\mu_{2D}(N_{2D} + N_1\mu_1/\mu_{2D}) \text{ (conductivity measurement)}, \quad (18)$$

where G is a geometrical factor for short-gate samples. In our cases, $\mu_1 \approx 10^3$cm^2/V sec while $\mu_{2D} \approx 10^5$ cm^2/V sec and N_1 never exceeds N_{2D} significantly, such that the condition for Eq. (17), $\mu_1 N_1 \ll \mu_{2D} N_{2D}$, holds. In both measurements of N_s and I_{SD}, the N_{2D} term contributes more than the N_1 term.

Since PPC and its associated decay produces a change in conductivity, not a net charging, a change in the number of free carriers is accompanied by a change in fixed charge. In the simplest decay case, when V_g is near V_t (and the $Al_xGa_{1-x}As$ layer is totally depleted), N_{2D} is small compared to the ionized donor density in the $Al_xGa_{1-x}As$ layer so that tunneling-assisted decay in N_{2D} does not strongly change N_i. This means μ_{2D} decreases from reduced screening with the net result being the decay of I_{SD}. When V_g is chosen so that the $Al_xGa_{1-x}As$ layer is not totally depleted, the observed decay in I_{SD} occurs partially from a decrease of low-mobility carriers via direct recapture to deep levels. Simultaneously N_{2D} self consistently decreases in order to satisfy the depletion approximation, as well as decaying by tunneling-assisted recombination. The decay in I_{SD} results from this combined decrease of N_1 and N_{2D} (although there may be weak increases in their mobilities[7,19]). Nevertheless, the overall relaxation behavior of

I_{SD} of N_s is mostly dependent on the capture energy and lifetime prefactors of the decay mechanisms and not strongly determined by details of the dependence of the mobilities on the charge state of the sample.

Given the persistence range of seconds to hours at the temperatures of interest here, most data were recorded between 0 and 1000 sec so that a decay-rate "window" of 1–500 sec is measured in our experiments. This includes what is sometimes referred to as the "transient" photocurrent regime, but we do not adopt this terminology since the selection of time window merely sets the temperature range for a given photoconductance process to manifest itself, as in deep-level transient spectroscopy.

The decay is nonexponential, as illustrated in Figs. 4(a) and 4(b) from a VDP dc measurement on sample *DD* at 77 K. The time window is 10^{-3}–10^{5} sec. Typically the source-drain current or VDP sheet density decays after brief white-light illumination and shows a fast initial decay, followed by a decay rate that decreases continuously as the decay approaches a base line above the dark value (the long-term PPC). The decay nearly behaves as a straight line when plotted as a function of $\log_{10}(t)$ over nearly 7 orders of magnitude in time. For convenience, the $K(t)$ value calculated in this experiment is with respect to $\log_{10}(t)$. In this way, a single-rate decay with an amplitude of N_{00} will correspond to an experimental result of $K(t)$ with a peak value of 0.85 $\times N_{00}$. The logarithmic time derivative of N_s is also plotted as a dashed curve in Fig. 4(b). The curve of $K(t)$ shows a single decay peak seen at $t=10$ msec, while

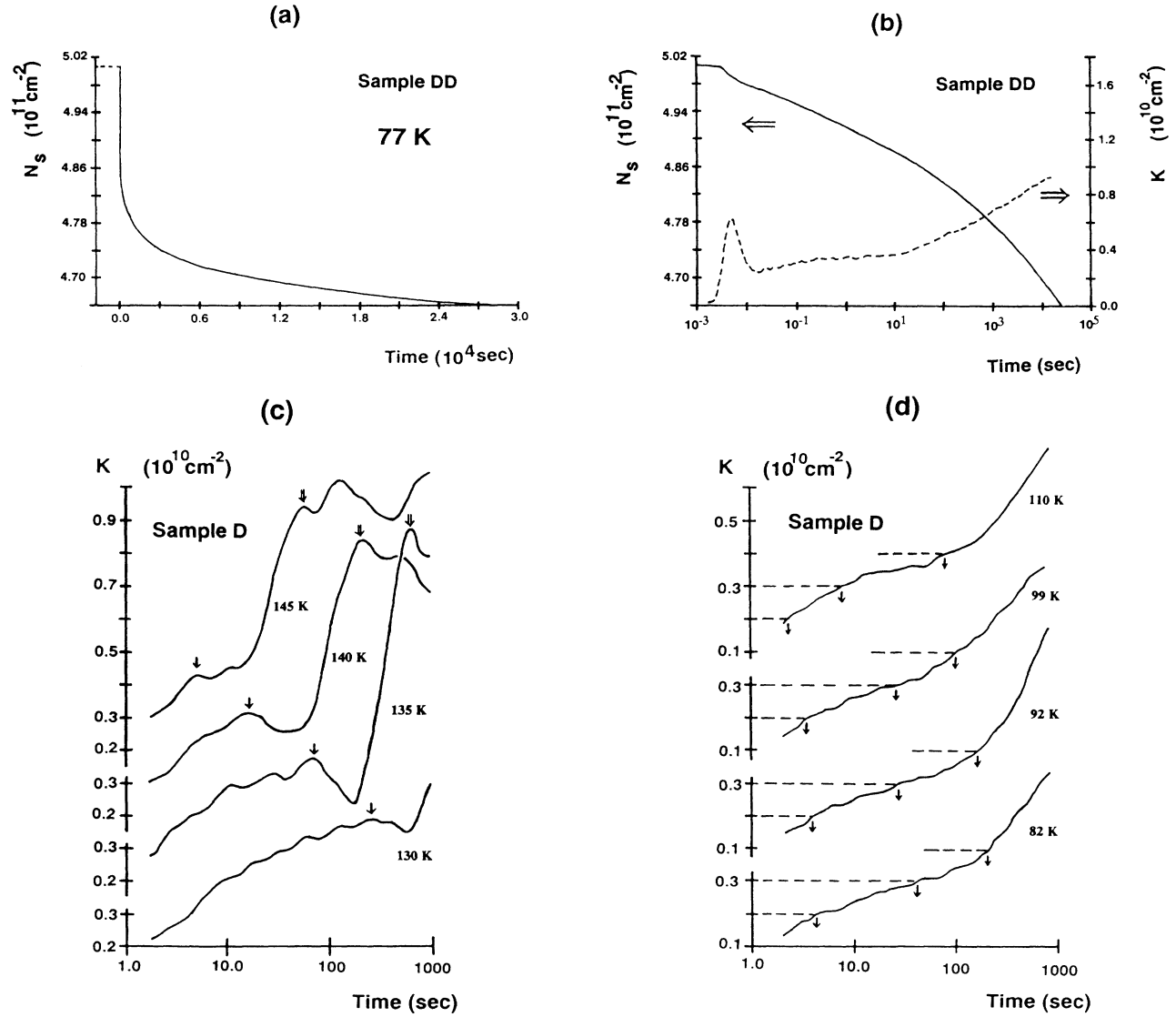

FIG. 4. (a) Nonexponential PPC decay from sample *DD* at 77 K over the 10^{-3}–10^{5}-sec rate window. It is plotted as a function of linear time. (b) The same decay plotted with logarithmic time. The value of $K(t)$ is also plotted as a dashed curve. (c) and (d) are examples of the experimental $K(t)$ data from an ungated van der Pauw square (sample *D*).

most of the curve is a slowly increasing base line over nearly 6 orders of magnitude in time. This behavior is consistent with the theoretical prediction of Fig. 3(b).

In repeated measurements following illumination sufficient to saturate I_{SD} or N_s, the $K(t)$-$\log_{10}(t)$ plot of the decay curve shows no significant shift of these features at the same temperature. Raising the temperature speeds up each decay, but as long as the temperature change is small enough, individual peaks or the structure of curves can be tracked. The shifts of the decay structures with changing T gives the characteristic activation energies of the individual decay features. Figure 4(c) shows the shifts of decay groups with temperature from the measurements of N_s on sample D (ungated). The broad individual decay peaks can easily be tracked on top of a slowly increasing base line in the 130–145-K temperature range. Notice that the peak values of $K(t)$ are nearly the same when they shift from different temperatures. The peak value of $K(t)$ is 1×10^{10} cm^{-2}, which corresponds [from formula (12) plus a factor of ln10=2.30] to 6×10^{10} cm^{-2} of directly captured electrons. From the temperature dependence of the peak shifts, we can deduce capture energies and lifetime prefactors. The capture energy of these peaks is measured to be 370 meV with a lifetime prefactor of 10^{-10} sec. By contrast, in Fig. 4(d) in the temperature range of 82–110 K, there is no obvious track of peak shifts, but a slowly increasing base-line structure becomes clear, whose overall horizontal shift at the same values of $K(t)$ can be tracked at different temperatures. The same value of $K(t)$ is marked on the decay curves taken at different temperatures. A similar method was used over the range of 145–180 K.

The track of the single decay peaks or the track of the slowly increasing base-line structure [see discussion following formula (11)] from sample D is shown in Fig. 5(a) and summarized in Table II. Figure 5(a) displays several distinct decay mechanisms at different temperature regimes, marked as (ii)–(iv). Over the temperature ranges of 80–125 K (iv), sample D shows a retrapping energy of 20–40 meV, with a prefactor value equal to about 1–100 sec indicating that tunneling into shallow donors is involved. Actually, the tunneling-assisted capture must have the same capture energy as that corresponding to direct capture by the same kind of ionized donor. However, the lifetime prefactor is much longer due to the small tunneling probability. The dominant activation energy increases to about 140 meV with a 10^{-4}-sec lifetime prefactor at higher temperatures $T=145$–180 K (ii) as deeper traps are involved after tunneling and as the macroscopic barrier width decreases due to a thermally induced increase of free carriers in the $Al_xGa_{1-x}As$ layer at higher temperatures.[20,21] This is consistent with the measurements (in the dark, or with illumination) on sample D and sample DD [to be discussed later in Fig. 7(b)] which show that the sheet number density is increasing rapidly when T is greater than 120 K but is nearly constant when T is below 110 K. In addition to tunneling-related retrapping back to deep and shallow donor centers, thermally activated behavior was detected over a narrow intermediate temperature range, as seen in the steep portions [marked (iii)] of Fig. 5(a). Sample D displays a retrapping energy of 370 meV with a 10^{-10}-sec prefactor over a narrow temperature range at 130–145 K [region (iii)], in sharp contrast with the factor-of-3 lower capture energy and 6-orders-of-magnitude longer prefactor at adjacent temperatures (ii) and (iv). Although sample D has an extra-high barrier in the spacer layer, the intermediate values of activation energy yet long (1–100 sec) lifetime prefactor of regions (iv) can be explained by tunneling of persistent photoelectrons between the GaAs cap layer and the adjacent $Al_xGa_{1-x}As$ layer ($x=0.30$), since the conduction band

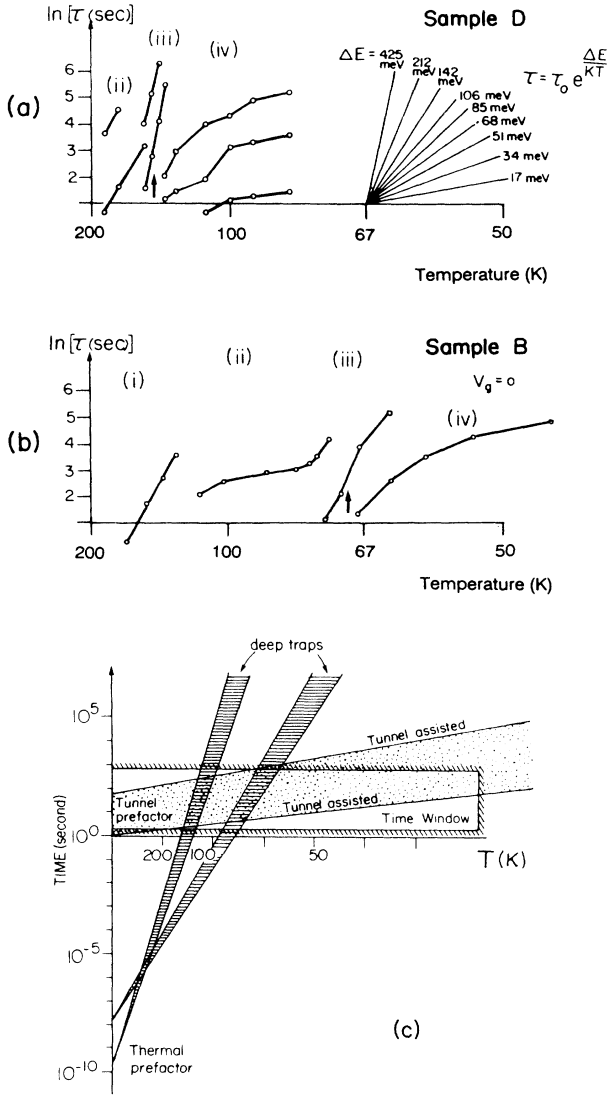

FIG. 5. Temperature dependence of peaks associated with groups of traps from multiple-rate trap spectroscopy. (a) Sample D; (b) sample B ($V_g=0$); (c) sketch of the dominant features of the above results. Data extracted from different samples in different temperature regions labeled in this figure are shown in Table II.

TABLE II. Data extracted from Fig. 5, including the labels of different sample and different temperature regions, the temperature range of the labeled region, the capture energy E_c, deviation of capture energies ΔE_c, and lifetime prefactors τ_0.

Sample	Label in figure	Temperature range (K)	E_c (meV)	ΔE_c (meV)	τ_0 (sec)
B ($x=0.3$)	(i)	120–160	150	20	10^{-4}
B	(ii)	80–120	30	20	5
B	(iii)	65–75	150	20	10^{-8}
B	(iv)	45–60	20	10	5
D ($x=0.3$)	(ii)	145–180	140	20	10^{-4}
D	(iii)	130–145	370	40	10^{-10}
D	(iv)	80–125	30	10	1–100

of the doped GaAs cap layer in this sample is closer to E_F than in the sketch of Fig. 1, and can hold photoexcited free carriers. Since DX centers in very heavily doped GaAs have been detected,[22,23] direct capture by a DX center can occur in a heavily doped cap layer. The results from ungated VDP sample L with a much wider and heavier doped GaAs cap layer and doped $Al_xGa_{1-x}As$ layer show that along with a slowly increasing base line with $K(t)\approx 2\times 10^{10}$ cm^{-2}, a large single decay peak due to direct recapture with $K(t)$ of the order of 4×10^{11} cm^{-2}, which is 40 times larger than the case of sample D, was observed and the reduced capture energy from the peak shifts is 350 meV in the temperature range 140–170 K.

An example from the conductivity measurements on sample B ($V_g=0$) shown in Fig. 5(b) also displays several distinct decay mechanisms in different temperature regimes, marked as (i)–(iv) and summarized in Table II. Over the temperature ranges of 45–65 K (iv) and 80–120 K (ii), sample B shows a retrapping energy of 15–50 meV, with a prefactor value equal to about 1 sec indicating that tunneling into shallow donors is involved. The dominant activation energy increases to about 150 meV at higher temperatures (i) as deeper traps are involved following tunneling and as the macroscopic barrier width decreases due to a thermally induced increase of free carries in the $Al_xGa_{1-x}As$ layer at higher temperatures. In addition to tunneling-related retrapping back to deep and shallow donor centers, thermally activated behavior was detected over a narrow intermediate temperature range, as seen in the steep portions [marked (iii)] of Fig. 5(b). Sample B displays a retrapping energy of 150 meV with a 10^{-8}-sec prefactor over a narrow temperature range at 65–75 K [region (iii)] in sharp contrast with the factor-of-8 lower capture energy and 8-orders-of-magnitude longer prefactor at adjacent temperatures (ii) and (iv). An ungated sample G from the same wafer shows a 170 meV capture energy at $T=80$ K, a slightly higher temperature than observed for gated samples. Sample C ($V_g=-0.8$ V) with $x=0.21$ also clearly displays this sharp kink signature of the high-activation-energy (200 meV) thermally activated process over a narrow temperature range of 65–75 K. The capture energy is 220 meV from sample C with $V_g=0$ over the same narrow temperature range. But for the same sample with V_g close to pinchoff ($V_g=-1.5V$), direct capture by an ionized donor was not observed.

All the dominant features from our samples can be summarized in Fig. 5(c). A high-activation-energy (150 or 370 meV) short-prefactor (10^{-8}–10^{-10} sec) process crosses through the experimental rate window over a narrow temperature range, intersecting a low-activation-energy, long-prefactor process which is visible in the data of Figs. 5(a) and 5(b) as lines of the small slope on either side of the steep-slope portion.

The key conclusion that qualitatively different decay channels may be separated using the $\ln(t)$-derivative technique can be verified in an alternative decay experiment shown in Fig. 6. A continuous temperature sweep

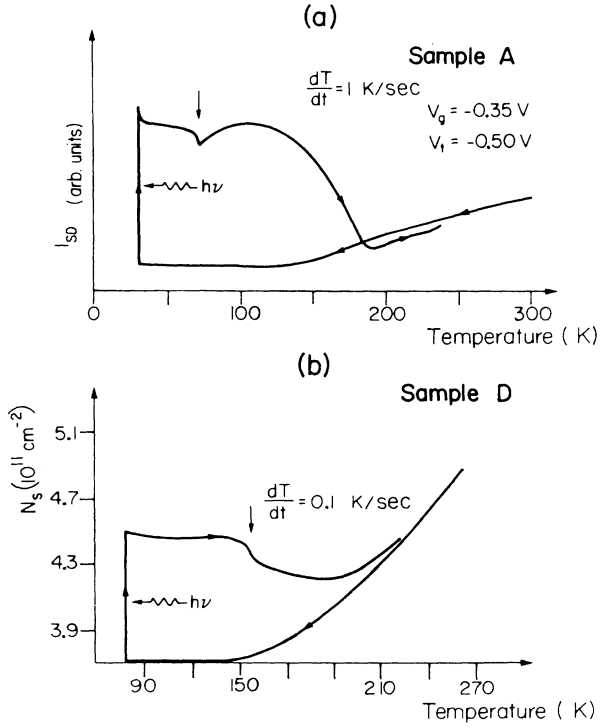

FIG. 6. Temperature-sweep method of observing elevated PPC decay at special temperatures (arrow) in (a) gated transistor structures and (b) Hall patterns.

at a constant rate of about 1 K/sec performed on sample A after illumination is shown in Fig. 6(a). I_{SD} shows a faster decay in the temperature interval near 70 K, in agreement with the kink portion observed in the data in Fig. 5(b) at a comparable temperature. The temperature at which the extra dip occurs of course shifts with sweep rate as in DLTS [shifting rate window in Fig. 5(c)] and is measured to be weakly gate-voltage dependent. A similar result is obtained for sample D in a temperature-sweep measurement of N_s [Fig. 6(b)] when the sample is warmed from 77 K at 0.1 K/sec after a brief white-light illumination. A sudden dip in number density is observed (see arrow) when T passes through 150 K, which agrees with the steep-slope portion of Fig. 5(a).

In this work, we have obtained three different apparent DX-center capture energies with different Al fractions: 370 meV for $x=0$, 220 meV for $x=0.21$, and 170 meV for $x=0.30$. When the energy differences between the L and Γ minima at different Al fractions are included,[6] the net capture barrier height in the local DX-center configuration coordinate model is 90 ± 30 meV for all samples we measured. This is in reasonable agreement with DLTS results for the emission barrier height (200–400 meV) and the fixed energy value (150 meV independent of x) by which the DX center is located below the L minimum of the conduction band.[7,13]

An example of a more complete picture of the tunneling-assisted multiple-rate decay is from dc VDP measurements [data shown in Fig. 7(a)] on sample DD (from the same wafer as sample D). The time window is set from 1 msec to 500 sec. To detect the decay in these short times, a light emitting diode (LED) is used for illumination and the instruments are set to have a 0–10 kHZ response. In the temperature range of 86–178 K, every curve shows a single decay peak (with a few msec lifetime) and is followed by a slowly increasing base line. The temperature dependence of the single short decay lifetime displays the behavior of shallow donors as above. The decay curve that follows can be fit to the numerical tunneling calculation of Fig. 3(b). Sample DD has an extra-high barrier between the $Al_xGa_{1-x}As$ and GaAs layers due to the aluminum ratio $x=1$ in the 10-nm spacer layer, which prevents tunneling through this barrier to be observed in our decay-rate window. Only the tunneling-assisted decay between the cap layer and the doped AlGaAs layer is detected. For simplicity, the measured change of the sheet number density is proportional to the change of the free carriers in the parallel conductance layer. From formula (17), the apparent value $K(t)$ from the measured sheet number density will be smaller than the real value due to capture in the parallel conductance layer. Nevertheless, the basic feature of tunneling-assisted decay can be clearly seen in the experimental results with the slowly increasing value of $K(t)$ and the decreasing tails when the depletion width becomes shorter at higher temperatures.

The dashed curves in Fig. 7(a) are the calculated results using the following parameters. The potential barrier height U_0 at the first ionized-donor layer is calculated from the conduction-band discontinuity (0.23 eV for $x=0.3$) at the 2D interface and the potential drop through the 10-nm undoped $Al_xGa_{1-x}As$ layer (Fig. 2). The potential drop from the 2D interface is readily calculated using the depletion approximation[24] resulting in

$$N_i e/2\epsilon=\Delta E_c(M^2d^2+2LMd)^{-1}\ , \tag{19}$$

$$U_0=N_i e/2\epsilon M^2d^2\ , \tag{20}$$

where ΔE_c is the conduction-band discontinuity at the 2D interface, ϵ is the dielectric constant ($\epsilon=13$ for our

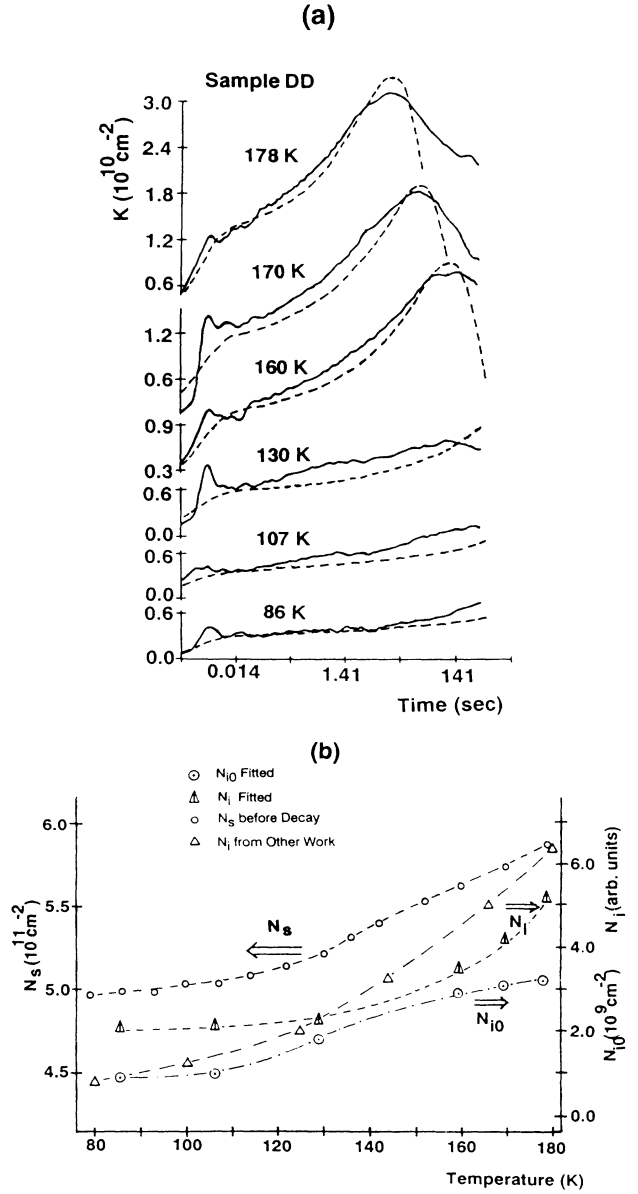

FIG. 7. (a) Experimental results (solid curves) of the tunneling-assisted capture from ungated VDP sample DD. Dashed curves are the calculated results from a realistic tunneling barrier. (b) The parameters N_{i0} and N_i used in the calculation of (a). The experimental data of the sheet number density N_s before each decay, and the temperature dependence of the bulk ionized-donor density N_i from other work is also presented.

TABLE III. The fitted values of N_{i0} (refilled electron density of a single donor-atom layer) and the fitted values of M (the total number of ionized donor-atom layers) from the data in Fig. 7(a). The ionized-donor densities N_i calculated from the value of M are also presented.

T (K)	N_{i0} (10^9 cm^{-2})	M	N_i (10^{17} cm^{-3})
86	0.9	105	2.27
107	1.0	104	2.30
130	1.9	102	2.38
160	2.9	78	3.61
170	3.1	70	4.25
178	3.3	61	5.21

case), L is the thickness of the undoped spacer layer, and M is the total number of ionized-donor-atom layers such that Md is the depletion width. From (19) and (20), we can calculate the value of U_0 and N_i by choosing the value of M. The lifetime of the tunneling-assisted capture into the first layer is selected to be 10 msec (the tunneling barrier in the undoped layer and the lifetime of a shallow donor are not very temperature sensitive). Using formulas (13), (15), and (16) for a fixed conduction-band discontinuity, the overall variation of $K(t)$ with time is determined by the ionized-donor density N_i (consequently the depletion width), but the amplitude of $K(t)$ is determined by the values of N_{i0}. The fitted values of N_{i0} and the corresponding values of M and N_i found from the fit at different temperatures are shown in Table III. The theoretical calculation fits the data fairly well, and the parameters are consistent with the doping density of 1×10^{18} cm^{-3}, which gives a maximum value of $N_i=1\times10^{18}$ cm^{-3} and a corresponding maximum $N_{i0}=2.8\times10^{10}$ cm^{-2}.

This variation in the fitting parameters N_{i0} and N_i requires a depletion width which increases with increasing temperature, which is consistent with the following independent check. The temperature dependence of the parameters N_{i0} and N_i used to fit data in Fig. 7(a) are shown in Fig. 7(b). The measured sheet number density N_s before each decay is also plotted for comparison. The value of N_s is generally an increasing function of N_i in the doped supply layer with increasing temperature, and Fig. 7(b) shows the same behavior for N_s and fitting parameters N_{i0} and N_i. In Fig. 7(b), the temperature dependence of the bulk $Al_xGa_{1-x}As$ ionized-donor density with an Al fraction of $x=0.34$ and doping density of 1.7×10^{17} cm^{-3} is also presented,[25] which also shows a similar temperature dependence.

IV. CONCLUSION

We have introduced a method for separating multiple-rate decay mechanisms in persistent photoconductivity (PPC) decay of GaAs/$Al_xGa_{1-x}As$ heterostructure. The derivative of the decay of measured conductivity, or carrier number density with respect to the logarithm of time shows a slowly varied base-line structure with some pronounced peaks. The temperature dependence of the varied base line agrees with the temperature dependence of the tunneling barrier. The temperature dependence of the base-line structure and the positions of the pronounced peaks were analyzed to yield two distinctly different classes of decay mechanisms: a high-activation-energy, short-prefactor time mechanism associated with the DX center in doped AlGaAs, and a low-activation-energy, long-prefactor mechanism associated with tunneling-assisted recombination of 2DEG electrons across the macroscopic barrier between GaAs and $Al_xGa_{1-x}As$.

The collected evidence from this work demonstrates that the combination of measured capture energies and lifetime prefactors can distinguish the microscopic mechanisms (direct capture) for PPC decay in the doped layer from other capture mechanisms. (1) The short-lifetime prefactor (10^{-8}–10^{-10} sec) and associated capture energies are in good agreement with results from other work on the DX-center capture mechanism.[11,19] These short-lifetime prefactors compare with prefactors longer by as much as 10 orders of magnitude at adjacent temperatures (Fig. 5), which can be identified as tunneling-related photoconductance decay of 2D electrons into shallow or deep donors in the AlGaAs layer. (2) The gate bias does not change the electric field within the GaAs buffer region. So the mechanism with a short-lifetime prefactor cannot lie on the GaAs side of the heterojunction because of the observed strong gate-bias dependence and the doping-density dependence of the decay magnitude.

ACKNOWLEDGMENTS

This work was supported by the National Science Foundation, Division of Materials Science (NSF-DMR) Grants No. 81-19550, No. 81-13456, and No. 85-19728, and by the Tektronix Foundation. It is a pleasure to thank K. R. Gleason (Tektronix), P. R. Jay and P. Delescluse (Laboratoire Central de Recherches, Thomson-CSF), W. Schaff (Cornell), and T. Hurl (Gain) for supplying useful samples and J. D. Cohen, M. N. Wybourne, and A. V. Gelatos (University of Oregon) for helpful discussions.

*Present address: School of Electrical Engineering, Georgia Institute of Technology, Atlanta, GA 30332.

[1]M. I. Nathan, Solid-State Electron. **29**, 167 (1986).
[2]D. E. Theodorou and H. J. Queisser, Appl. Phys. **23**, 121 (1980).
[3]E. F. Schubert, A. Fischer, and K. Ploog, Phys. Rev. B **31**, 7937 (1985).
[4]D. V. Lang and R. A. Logan, Phys. Rev. Lett. **39**, 635 (1977).
[5]D. V. Lang and R. A. Logan, Phys. Rev. B **19**, 1015 (1979).
[6]A. K. Saxena, Solid-State Electron. **25**, 127 (1982).

[7]N. Chand, T. Henderson, J. Klem, W. T. Masselink, R. Fischer, and H. Morkoç, Phys. Rev. B **30**, 4481 (1984).
[8]M. Mizuta, M. Tachikawa, H. Kukimoto, and S. Minomura, Jpn. J. Appl. Phys. **24**, L143 (1985).
[9]P. M. Mooney, E. Calleja, S. L. Wright, and M. Heiblum, in *Proceedings of the 14th International Conference on Defects in Semiconductors,* edited by H. J. von Bardeleben (Trans Tech, Switzerland, 1987), Vols. 10–12, p. 417.
[10]E. Calleja, P. M. Mooney, S. L. Wright, and M. Heiblum, Appl. Phys. Lett. **49**, 657 (1986).
[11]P. M. Mooney, N. S. Caswell, P. M. Solomon, and S. L. Wright, Mater. Res. Soc. Symp. Proc. **46**, 403 (1985).
[12]M. O. Watanabe, K. Morizuka, M. Mashita, Y. Ashizawa, and Y. Zohta, Jpn. J. Appl. Phys. **23**, 103 (1984).
[13]P. M. Mooney, R. Fischer, and H. Morkoç, J. Appl. Phys. **57**, 1928 (1985).
[14]H. J. Queisser and D. E. Theodorou, Phys. Rev. B **33**, 4027 (1986).
[15]A. D. N. Swingler, IEEE Trans. Biomed. Eng. **BME-24**, 408 (1977).
[16]R. Fischer, T. J. Drummond, J. Klem, T. Henderson, D. Perrachione, and H. Morkoç, IEEE Trans. Electron Devices **ED-31**, 1028 (1984).
[17]J. P. Harrang, R. J. Higgins, R. K. Goodall, R. H. Wallis, P. R. Jay, and P. Delescluse, J. Appl. Phys. **58** (1985).
[18]J. P. Harrang, Ph.D. thesis, University of Orgeon, 1984.
[19]R. J. Nelson, Appl. Phys. Lett. **31**, 351 (1977).
[20]T. J. Drummond, W. Kopp, R. Fischer, H. Morkoç, R. E. Thorne, and A. Y. Cho, J. Appl. Phys. **53**, 1238 (1982).
[21]E. F. Schubert and K. Ploog, Phys. Rev. B **30**, 7021 (1984).
[22]P. M. Mooney, Bull. Am. Phys. Soc. **32**, 504 (1987).
[23]M. I. Nathan, M. Heiblum, T. N. Morgan, L. Eaves, D. K. Maude, J. C. Portal, R. B. Beall, and J. J. Harris, Bull. Am. Phys. Soc. **32**, 553 (1987).
[24]T. J. Drummond, W. T. Masselink, and H. Morkoç, Proc. IEEE **74**, 777 (1986).
[25]M. O. Watanabe and H. Maeda, Jpn. J. Appl. Phys. **23**, L734 (1984).